Proceedings of the Conference on Computational Engineering and Science JSCES
Vol. 29, Jun. 2024

Smoothed Particle Hydrodynamics simulation of landslides with discontinuities

Daniel S. Morikawa [1)] and Mitsuteru Asai [2)]

[1)] Ph.D., JAMSTEC (3173-25, Showa-machi, Kanazawa-ku, Yokohama-city, Kanagawa, E-mail: morikawad@jamstec.go.jp)
[2)] Ph.D., Kyushu University (819-0395, 744 Motooka Nishi-ku, Fukuoka, E-mail: asai@doc.kyushu-u.ac.jp)

This study presents a novel approach for simulating geotechnical problems including the initiation and post-failure behavior of discontinuities. The developed method is constituted by a mixed total Lagrangian–updated Lagrangian Smoothed Particle Hydrodynamics (SPH) method, which the main characteristic is to distinguish between internal forces within a body and contact forces from interactions with other bodies as internal stress and collision stress, respectively. Internal stress effects are calculated using total Lagrangian SPH interpolations, while collision stress effects are computed with updated Lagrangian. Fractures are simulated by employing plastic deformation as a damage measure, with fully damaged particles detached from their original body and treated as a separate particulate material, interacting via collision stress.

Key Words : *Landslide, Slope stability, Smoothed particles hydrodynamics, Discontinuities*

1. INTRODUCTION

Smoothed Particle Hydrodynamics (SPH) has emerged as a versatile numerical method for simulating astrophysical problems [1,2], and it is currently used in various applications. Unlike grid-based methods, SPH represents the materials with discrete Lagrangian particles, allowing for efficient and accurate modeling of large deformations.

Under this premise, several researchers have used the SPH method for landslide simulations such as [3,4,5] and others. However, the appearance of a discontinuities within the soil mass as the detachment of the landslide mass happens is still a great challenge.

The primary objective of this study is to introduce a novel SPH method capable of simulating post-failure behavior of fractured soil masses including self-contact interactions. By integrating the stability and accuracy of the total Lagrangian framework with the adaptability of the updated Lagrangian, our method aims to accurately represent the complex interactions between intact and fractured regions within a soil mass during landslide events.

2. THE SPH METHOD

The SPH method is a Lagrangian meshless particle method in which functions are approximated according to neighboring particles [1,2]. The classical equation for the the approximation of a generic function f can be written as

$$\langle f \rangle_i = \sum_j \frac{m_j}{\rho_j} f_j W(\mathbf{r}_{ij}, h), \tag{1}$$

where i and j stands for target and a neighbor particles, respectively, m the mass, ρ the density, $\mathbf{r}_{ij} = \mathbf{x}_i - \mathbf{x}_j$ the relative position vector, W the weight function (also called kernel) and h the smoothing length. In this study, we selected the cubic spline kernel.

In most of SPH applications, the most relevant SPH operators are the spatial derivatives. In the current work, we use corrected versions of ∇f developed by [6,7,8] that improves the accuracy of the first derivative evaluation. Such equations are shown in details for each operator used in the next sections.

3. FORMULATION

Let us formulate the governing equations using Fig. 1 to illustrate a body under consideration following the premises of continuum mechanics. The body can be described either by its reference configuration (volume Ω_0 and surface Γ_0), with position vector $\mathbf{X}$, or deformed configuration (volume Ω and surface Γ), with position vector $\mathbf{x}$. The position vectors are associated by the deformation gradient. The body may be subjected to prescribed velocity Dirichlet boundary conditions at Γ_v ($\mathbf{v} = \bar{\mathbf{v}}_0$, where $\mathbf{v}$ is the velocity vector), volumetric forces $\mathbf{b}$ and external *boundary forces*. Such boundary forces may be represented as prescribed forces represented by $\bar{\mathbf{t}}$ (or $\bar{\mathbf{T}}$) at Γ_t or by contact forces with an outer body represented by $\mathbf{t}_\mathrm{c}$ (or $\mathbf{T}_\mathrm{c}$) at Γ_c. Finally, under deformation, the body presents *internal forces* resulting from interactions between adjacent body parts, represented by a traction vector $\mathbf{t}_\mathrm{i}$ (or $\mathbf{T}_\mathrm{i}$). Notice that we may use the notation of capital letters or the subscript index "0" to represent the reference configuration, depending on the case.

Internal forces $\mathbf{t}_\mathrm{i}$ (or $\mathbf{T}_\mathrm{i}$) and boundary forces $\mathbf{t}_\mathrm{c}$ and $\bar{\mathbf{t}}$ (or $\mathbf{T}_\mathrm{and}$ and $\bar{\mathbf{T}}$) are collectively known as *surface forces* [9], and, following Cauchy's Theorem, the body forces of the material may be represented by a second order vector called Cauchy stress $\boldsymbol{\sigma}$ such that $\mathbf{t} = \boldsymbol{\sigma} \cdot \mathbf{n}$. A similar equation can be derived using the reference configuration as $\mathbf{T} = \mathbf{P} \cdot \mathbf{n}_0$, where $\mathbf{P}$ is the nominal stress.

As explained before, the traction vector may be de-

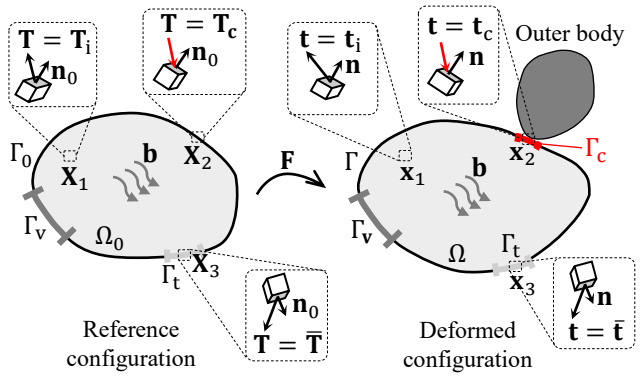

Fig. 1 Schematic illustration of reference and deformed configurations and traction vectors for internal and collision stresses

composed into internal forces $\mathbf{t}_\mathrm{i}$, contact forces $\mathbf{t}_\mathrm{c}$ and prescribed boundary forces $\bar{\mathbf{t}}$. Therefore, applying the Cauchy's Theorem for the contact forces, we define the *contact stress* $\boldsymbol{\sigma}_\mathrm{c}$ as

$$\mathbf{t}_\mathrm{c} = \boldsymbol{\sigma}_\mathrm{c} \cdot \mathbf{n}. \tag{2}$$

The concept of contact stress has been first described by Hertz in 1882 [10,11], and it is one of the key concepts for the field of contact mechanics. We do not define the nominal stress for the contact forces because we do not use it in our proposed method. In addition, we denote the stress tensor for the internal forces $\mathbf{t}_\mathrm{i}$ simply as $\boldsymbol{\sigma}$ (or $\mathbf{P}$), for simplification.

(1) Governing equations

Applying the conservation of linear momentum to a body subjected to all conditions described previously, decomposing the traction vector as $\mathbf{t} = \mathbf{t}_\mathrm{i} + \mathbf{t}_\mathrm{c}$ (we ignore $\bar{\mathbf{t}}$, since we do not use prescribed boundary forces in this method, although its inclusion is trivial), using the Gauss's Theorem, transforming into the strong form and rearranging, we derive

$$\frac{D\mathbf{v}}{Dt} = \frac{1}{\rho}\nabla \cdot \boldsymbol{\sigma} + \frac{1}{\rho}\nabla \cdot \boldsymbol{\sigma}_\mathrm{c} + \mathbf{b}, \tag{3}$$

where D/Dt is the material time derivative.

In the current work, we use the total Lagrangian form, i.e., the reference configuration, to calculate the acceleration caused by $\boldsymbol{\sigma}$, while using the updated Lagrangian form, i.e., the current configuration, for $\boldsymbol{\sigma}_\mathrm{c}$. Also, using ρ_0 is easier than ρ, since ρ_0 is a prescribed value that does not evolve with time. Therefore, we may rewrite Eq. (3) as

$$\frac{D\mathbf{v}}{Dt} = \frac{1}{\rho_0}\nabla_0 \cdot \mathbf{P} + \frac{1}{\rho_0}\nabla \cdot \boldsymbol{\tau}_\mathrm{c} + \mathbf{b}, \tag{4}$$

where $\boldsymbol{\tau}$ is the Kirchoff stress, and J is the Jacobian of $\mathbf{F}$.

In addition, the evolution of the deformation gradient can be defined as [9]

$$\frac{D\mathbf{F}}{Dt} = (\nabla_0 \otimes \mathbf{v})^T. \tag{5}$$

(2) SPH interpolations

The current method considers that some of the neighboring particles may be included for the calculation of total Lagrangian quantities, while others for updated Lagrangian ones. Therefore, the current section explains the neighboring search criterion to defined whether a neighboring particle should be included in $\mathbb{T}$ (neighboring in total Lagrangian framework) or $\mathbb{U}$ (neighboring in updated Lagrangian framework). Considering a target particle i, a particle j may be consider a neighboring particle in $\mathbb{T}$ if:

$$\mathbb{T}_i \equiv \{j = 1, 2, ..., N \ \mid \ R_{ij} < h_\mathrm{inf} \wedge \\ j \in \Omega_i \ \wedge \ D_i, D_j < 1\}. \tag{6}$$

This description considers the damage variable D which is explained in more details in the following section 3.(4).

Accordingly, a particle j belongs to $\mathbb{U}$ if:

$$\mathbb{U}_i \equiv \{j = 1, 2, ..., N \ \mid \ r_{ij} < h_\mathrm{inf} \wedge \\ (j \notin \Omega_i \ \vee \ D_i = 1 \vee D_j = 1 \ \vee \ R_{ij} > 2h_\mathrm{inf})\}. \tag{7}$$

The last condition takes into account self-contact between non fractured particles. Also, notice that the abovementioned conditions for $\mathbb{U}$ exclude any neighboring particle in $\mathbb{T}$, so there will be no double counting of neighbors. In the above definitions, $\mathbf{R}$ is the relative position vector at the reference configuration ($\mathbf{R}_{ij} = \mathbf{X}_i - \mathbf{X}_j$, $R_{ij} = |\mathbf{R}_{ij}|$)

With the above definitions, it is now possible to apply the SPH interpolations for the operators described in section (1). However, we first define the gradient correction in order to contemplate neighboring particles in both $\mathbb{T}$ and $\mathbb{U}$:

$$\tilde{\nabla} W_{ij} = \mathbf{L}_i \nabla W_{ij} \ ; \ \tilde{\nabla}_0 W_{ij} = \mathbf{L}_i \nabla_0 W_{ij} \tag{8}$$

$$\mathbf{L}_i = \\ \Big(\sum_{j \in \mathbb{T}_i} \frac{m_j}{\rho_j} \nabla_0 W_{ij} \otimes \mathbf{R}_{ji} + \sum_{j \in \mathbb{U}_i} \frac{m_j}{\rho_j} \nabla W_{ij} \otimes \mathbf{r}_{ji} \Big)^{-1}. \tag{9}$$

Next, we apply Eqs. (8) to the necessary operators. Since this topic is general knowledge in the SPH community, we simply list the main operators used in this study. To avoid repetition, we refrain from rewriting the same equations in the reference configuration, given the conversion can be done by simply substituting $\mathbb{U}_i$ with $\mathbb{T}_i$ and ∇ with ∇_0.

- Divergence of stress (either $\mathbf{P}$ or $\boldsymbol{\tau}_\mathrm{c}$):

$$\langle \nabla \cdot \boldsymbol{\tau} \rangle_i = \sum_{j \in \mathbb{U}_i} \frac{m_j}{\rho_j} \Big(\tilde{\nabla} W_{ij} \cdot \boldsymbol{\tau}_i - \tilde{\nabla} W_{ji} \cdot \boldsymbol{\tau}_j \Big). \tag{10}$$

- Gradient of velocity:

$$\langle \nabla \otimes \mathbf{v} \rangle_i = \sum_{j \in \mathbb{U}_i} \frac{m_j}{\rho_j} \tilde{\nabla} W_{ij} \otimes (\mathbf{v}_j - \mathbf{v}_i). \tag{11}$$

(3) Finite strain elastoplasticity

The Hencky model is an extension of the Hookean law to finite strain theory. Therefore, the stress (in this case,

the Kirchoff stress) has a linear relationship with the logarithmic strain as

$$\boldsymbol{\tau} = \mathbf{C}_{el} : \boldsymbol{\epsilon}, \tag{12}$$

$$\boldsymbol{\epsilon} = \frac{1}{2} ln\mathbf{B}, \tag{13}$$

where $\mathbf{C}_{el}$ is the tangent modulus for the Hookean material, ϵ is the logarithmic strain, and $\mathbf{B} = \mathbf{F} \cdot \mathbf{F}^T$ is the left Cauchy-Green strain tensor. Notice that the symbol *ln* in Eq. (13) refers to the tensor logarithmic operation. As usual, $\mathbf{C}_{el}$ is described by elastic parameters Young's modulus E and Poisson ratio ν (or equivalently shear modulus μ and bulk modulus K).

The current method is based on the multiplicative split between elastic and plastic deformation gradients ($\mathbf{F} = \mathbf{F}^e \cdot \mathbf{F}^p$). Using the logarithmic strain and some logarithm properties, it is straightforward to derive that $\boldsymbol{\epsilon} = \boldsymbol{\epsilon}_e + \boldsymbol{\epsilon}_p$. In this way, using the Hencky model and a conventional return mapping algorithm, we update the stress as

$$\boldsymbol{\tau}^{n+1} = \boldsymbol{\tau}^{\text{trial}} - \Delta\gamma \mathbf{C}_{el} : \mathbf{N}^{n+1}, \tag{14}$$

where $\Delta\gamma$ is the plastic multiplier, $\mathbf{N}$ is the direction of the plastic flow, and the superscript "trial" refers to a trial state of the stress. To obtain $\boldsymbol{\tau}^{\text{trial}}$, we have

$$\boldsymbol{\tau}^{\text{trial}} = \mathbf{C}_{el} : \boldsymbol{\epsilon}^{\text{trial}}, \tag{15}$$

$$\boldsymbol{\epsilon}^{\text{trial}} = \frac{1}{2} ln\mathbf{B}^{\text{trial}}, \tag{16}$$

$$\mathbf{B}^{\text{trial}} = \Delta\mathbf{F} \cdot \mathbf{B}^n \cdot \Delta\mathbf{F}, \tag{17}$$

$$\Delta\mathbf{F} = \mathbf{I} + \Delta t (\nabla_0 \otimes \mathbf{v})^T \cdot (\mathbf{F}^n)^{-1}. \tag{18}$$

As for the contact stress, we consider that it has a similar behavior as the internal stress with the exception that it does not produce traction forces. However, since the contact stress is calculated using the updated Lagrangian framework, $\Delta\mathbf{F}_{\text{c}}$ must be calculated as

$$\Delta\mathbf{F}_{\text{c}} = \mathbf{I} + \Delta t (\nabla \otimes \mathbf{v})^T. \tag{19}$$

After that, given that we are dealing with non-bounding collisions, positive values of the contact stress in the principal directions after the return mapping are eliminated as follows

$$\boldsymbol{\tau}_{c,k}^{n+1} = 0, \text{ if } \boldsymbol{\tau}_{c,k}^{\text{trial}} - \Delta\gamma \mathbf{C}_{el} : \mathbf{N}^{n+1} > 0. \tag{20}$$

(4) Fracture initiation

In this study, we consider the simplest and most classical approach to calculate fracture initiation, the so-called *strength hypotheses*. According to this concept, a fracture may be initiated if the material is subjected to a determined stress condition above its plastic yielding. Therefore, we define a damage variable using the plastic deformation as follows

$$D = \epsilon_p / \epsilon_{\text{limit}} \leq 1, \tag{21}$$

where ϵ_p is the plastic deformation, which depends on the yield criterion used and ϵ_{limit} is a material parameter that defines the amount of plastic deformation before fracture initiation.

In our study, as explained in section 3.(2), particles that undergo to a full damage condition (that is, $D_i = 1$) are considered as fractured particles, so they behave as a separated body. In this case, its internal stress is erased ($\boldsymbol{\tau}_i = \mathbf{P}_i = 0$), and its interaction with surrounding particles are limited to the contact stress.

4. NUMERICAL TESTS

(1) Brazilian test

The Brazilian test is one of the most standard experiments to determine the tensile strength of a material. It consists of a cylindrical material sample placed sideways between two plates that exert a compressive force on the sample. Given a sample of radius R and length L without a hole, and considering that the sample fractured at peak force P, the tensile strength of the material is given by $\sigma_t = \frac{P}{\pi R L}$.

The equation above considers that the material is brittle and its strength depends only on its tensile stress (that is, disregarding shear and compressive failures). Therefore, we have chosen a simple yield criterion that considers only the higher principal stress σ_1 to describe its plastic behavior. We follow the same material parameters as the physical experiment described in [12,13], which, among other parameters, are: $d = 5\times\ 10^{-4}$ m; $\Delta t = 1\times\ 10^{-8}$ s; $\rho =$ 2700 kg/m^3; $E = 49$ GPa; $\nu = 0.49$;$\sigma_t = 3.6$ MPa.

To compare with [12]'s results, we have simulated six models with different values of internal radius r for a hole placed in the center of the sample, and to simulate a brittle fracture, we set the plastic deformation limit ϵ_{limit} as 0.01 %. Gravity acceleration is ignored and the compressive plates are fixed with a velocity of 0.1 m/s.

Fig. 2 shows the resulting simulation for various values of r/R at the beginning ($\varepsilon = 0$) and end of the simulation ($\varepsilon = 0.005\%$). Here, the compressive strain ε is calculated as $\varepsilon = y_p/2R$, where y_p is the displacement of the compressive plates. Qualitatively, the simulation was fairly successful, since it could reproduce the fact observed in [12] that secondary horizontal cracks appears in samples with larger inner holes. The secondary cracks are also responsible for the appearance of a second peak in the evolution of P over time for samples with larger r/R, as shown in Fig. 3. Finally, we compare our results of maximum P for different values of r/R with the experimental results, showing a very good agreement between them.

(2) Triaxial compression test

This numerical example is the most important validation test, since our purpose with the study is to develop a numerical method for geomaterials in which the fractured material keeps in contact with the original mass. The triaxial compression test is a well-known experiment where a cylindrical sample is placed standing on a fixed base, and the upper surface is compressed by a cap. The sample is then loaded in all directions with a fixed water pressure p_0, and the side surface is protected by a rubber flexible

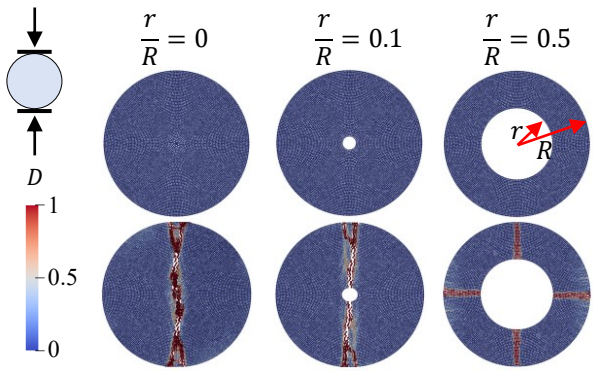

Fig. 2 Brazilian test: snapshot of simulation results for different values of r/R at $\varepsilon = 0$ and $\varepsilon = 0.005\%$

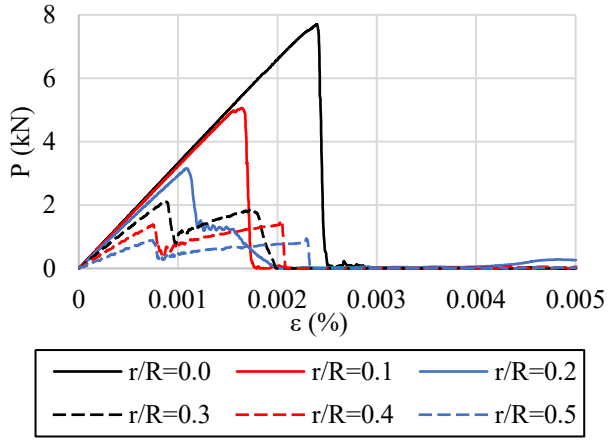

Fig. 3 Brazilian test: graph of P over ε for different values of r/R

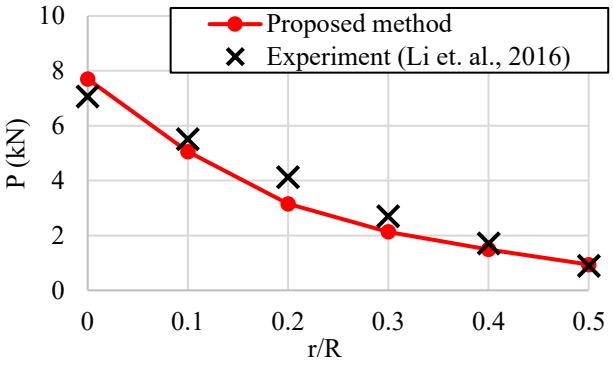

Fig. 4 Brazilian test: graph of maximum P over r/R in comparison with experimental results [12]

material to avoid the water to infiltrate into the sample. To model this rubber material and the fixed pressure, we placed ghost particles around the sample that moves with the same velocity as the closest sample particle and fixed with a collision stress of $\boldsymbol{\sigma}_c = p_0\mathbf{I}$. The geometrical and material parameters are the same as [14]: height= 10 cm; diameter= 5 cm; $d = 1\times 10^{-3}$ m; $\Delta t = 2\times 10^{-6}$ s; $\rho = 1530$ kg/m^3; $E = 3.1464$ MPa; $\nu = 0.2$; $\varphi = 30.5^o$. Gravity is neglected and the yield criterion is the Mohr–

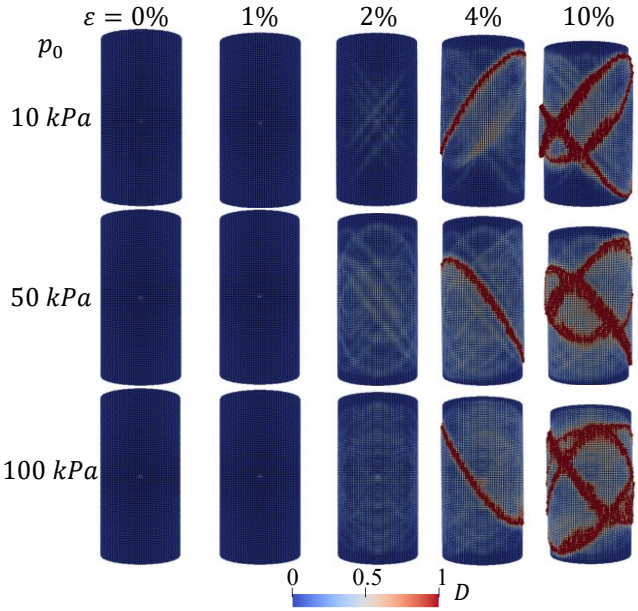

Fig. 5 Triaxial compression test: snapshots of simulation results for different values of p_0 and ε

Coulomb with $\epsilon_{\text{limit}} = 0.1$.

Although [14] has used a single value of cohesion for all of their numerical tests, we used a different value for each simulation, since its value can be obtained by analyzing the Mohr circle resulting from the residual value of q ($q = \sigma_y - p_0$, where σ_y is the stress in vertical y direction), that is, c should follow

$$(\sigma_y - p_0) - (\sigma_y + p_0)\sin\varphi - 2c\cos\varphi = 0. \quad (22)$$

Using the values of residual q observed in their physical experiment as 50, 126 and 230 kPa for the cases of $p_0 =$ 10, 50 and 100 kPa [14], we derive the values of cohesion as 8.4, 6.5 and 6.8 kPa, respectively. Notice that here we consider positive stress as compression in order to show the results in a familiar style for soil mechanics. In our numerical tests, we calculate the value of q as the force of the sample applied to the cap divided by the upper surface area minus p_0.

Fig. 5 shows the simulation for different values of p_0 and $\varepsilon = h_c/H$, where h_c is the displacement of the cap and H is the height of the sample initially. As expected, the resulting shear band follows an approximately 50^o of inclination. The evolution of q also follows a similar pattern in comparison to the experimental results from [14], as shown in Fig. 6. However, we observed a large peak value of q at the initiation of the plastic phase in our results, as well as some sudden drops in between. Such sudden drops reflect the initiation of a new fracture and the release of stress in the process.

In our opinion, it would be necessary to use a different constitutive model such as the Cam–Clay model in order to correctly reproduce the graphical results of Fig. 6. Since the scope of this work is to enable stable simulations of post-failure materials, we consider that this numerical test was successful.

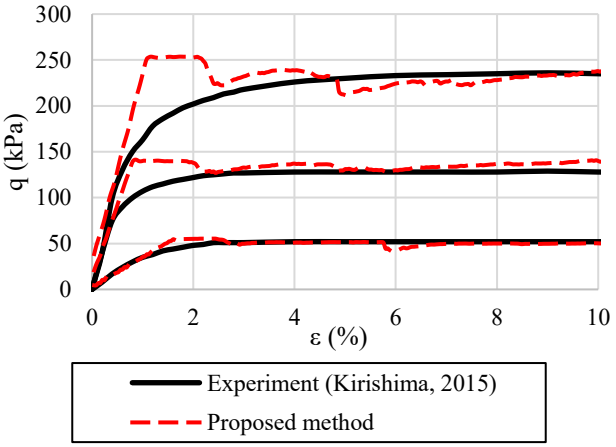

Fig. 6 Triaxial compression test: graph of q over ε for different values of p_0 in comparison with experimental results [14]

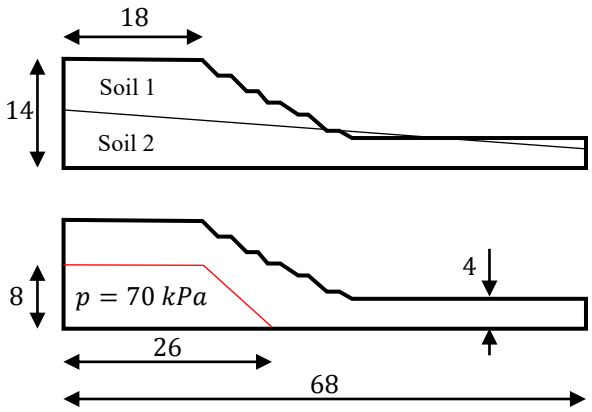

Fig. 7 Selborne experiment: model geometry and initial pressure condition following [15] (lenghts in m)

(3) Selborne experiment

The last numerical example is to show an application of the current method to a real world problem. Here, we consider the famous Selborne experiment [15], where a saturated soil slope of $1:2$ is loaded with a water pressure at the bottom of the slope, so that a landslide is observed at the water pressure of $p = 70$ kPa. The model geometry and pressure boundary condition is illustrated in Fig. 7. Previously [4], we have already successfully simulated this problem. Yet, in the current work, we demonstrate that the proposed method is capable of improving the previous result by generating a clear discontinuity in the soil mass, as observed in the real experiment.

Here, the 25 m wide soil slope is divided into two strata, weathered gault clay and unweathered gault clay, as shown in Fig. 7. We have simulated this problem with two particle sizes, and the other parameters are the same as the ones used in [4]. To simulate the current problem, we included a soil-water coupling technique based on the $\mathbf{u} - \mathbf{w} - p$ Biot's formulation in the same way as in [4]. Please refer to this paper, if the reader is interested in understanding the details of this formulation.

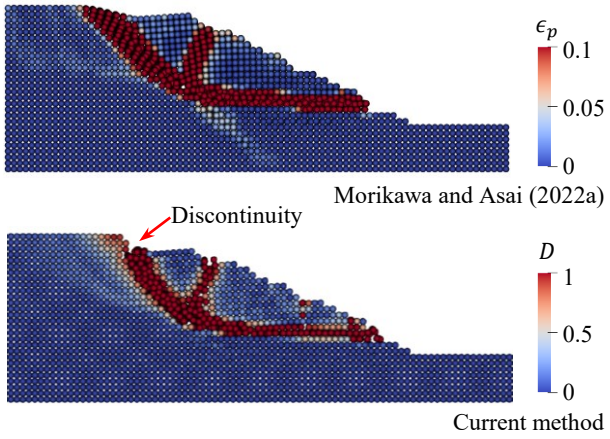

Fig. 8 Selborne experiment: comparison of the simulation result at $t = 50$ s between the proposed method and our previous results [4] ($d = 0.5$ m)

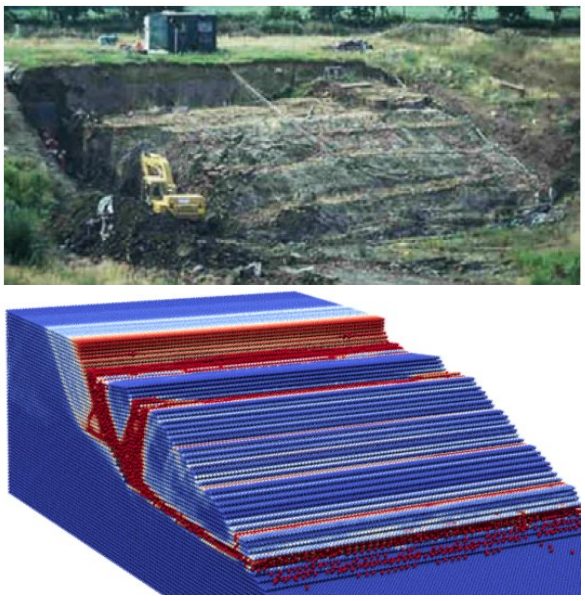

Fig. 9 Selborne experiment: comparison between observed photo from [15] and simulation at $t = 50$ s in a 3D view

First, we show the capability of our method in reproducing clear discontinuities. Fig. 8 shows a snapshot of the simulation at $t = 50$ s comparing our results with [4] using the same particle diameter ($d = 0.5$ m). In addition, we show a comparison between the a photo from [15] and our simulation in Fig. 9 (with $d = 0.25$ m). From these two figures, it is clear that our current results are more realistic in the sense that it reproduces the actual phenomenon of the detachment of the soil mass during the landslide.

For completeness, we also present a comparison between the observed shear band [15] and our simulation (with $d = 0.25$ m at $t = 1$ s) in Fig. 10. From this figure, it is clear that our results are reasonably in agreement with the observed experiment.

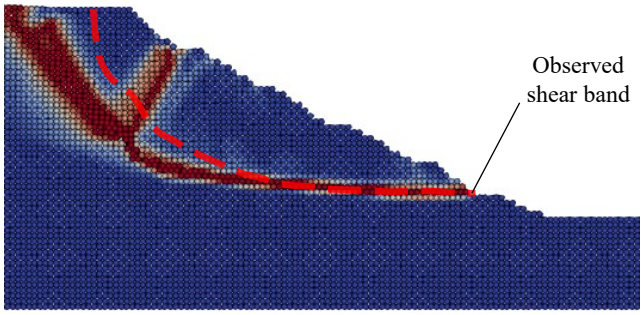

Fig. 10 Selborne experiment: comparison between damage profile of the soil at $t = 1$ s and the approximate observed slip surface from [15]

5. Conclusions

In this work, we have developed a mixed total Lagrangian–updated Lagrangian SPH method to simulate geomechanics problems with clear discontinuities. The core idea of the proposed method is to separate the internal forces within a body and the contact forces from the interaction with other bodies as an internal stress and a collision stress, respectively. In this way, the effects of the internal stress is calculated using total Lagrangian SPH interpolations, while the effects of the collision stress with updated Lagrangian. Finally, to simulate fractures, we propose to use the plastic deformation as a measure of damage, so that fully damaged particles are detached from its previous body and are considered a separated particulate material (therefore, their interaction being calculated with the collision stress).

As for the numerical tests, we validated the method for tension and shear fracture problems by simulating the famous Brazilian test adn the triaxial compression tests, showing good agreements with the experiments both in qualitative and quantitative terms. Lastly, we showed an application of the method to a real scale landslide scenario with the Selborne experiment. The results were reasonable in comparison with the observed experiment, showing a clear discontinuity in the shear band region.

In conclusion, we successfully accomplished the main goal of simulating the initiation of fractures and its following post failure behavior. We are aware that the methods to model the initiation of fractures used in this work are generally simplistic, so usage of more elaborate methods such as phase-field may be a next target for future works.

ACKNOWLEDGMENTS: This work was supported by the Japan Society for the Promotion of Science (JSPS) KAKENHI Grant Number JP- 23KK0182, 23H01662 and 22H03601. We also received computational environment support through the Joint Usage/Research Center for Interdisciplinary Large-scale Information Infrastructures (JHPCN) in Japan (Project ID: jh240032-NAH and jh230021-NAH).

REFERENCES

[1] Lucy, L.B.: A numerical approach to the testing of the fusion process, Astron. J., Vol.82, pp.1013-1024, 1977.
[2] Gingold, R.A. and Monaghan, J.J.: Smoothed Particle Hydrodynamics: theory and application to non-spherical stars, Astron. Soc., Vol.181, pp.375-389, 1977.
[3] Bui, H. and Nguyen, G.: A coupled fluid-solid SPH approach to modelling flow through deformable porous media, Int. J. Solids Struct., Vol.125, pp.244–264, 2017.
[4] Morikawa, D. and Asai, M.: Soil-water strong coupled ISPH based on u-w-p formulation for large deformation problems, Comput. Geotech., Vol.142, 2022.
[5] Morikawa, D.S., Asai, M.: A phase-change approach to landslide simulations: Coupling finite strain elasto-plastic TLSPH with non-Newtonian IISPH, Comput. Geotech., Vol.148, 104815, 2022.
[6] Randles, P. and Libersky, L.: Smoothed particle hydrodynamics: some recent improvements and applications, Comput. Methods Appl. Mech. Engrg., Vol.139, pp.375–408, 1996
[7] Bonet, J. and Lok, T.S.: Variational and momentum preservation aspects of smoothed particle hydrodynamics formulations. Comput. Methods Appl. Mech. Engrg., Vol.180, pp.97–115, 1999.
[8] Ganzenmuller, G.: An hourglass control algorithm for lagrangian smooth particle hydrodynamics. Comput. Methods Appl. Mech. Engrg., Vol.286, pp.87–106, 2015.
[9] Neto, E.S., Peric, D. and Owen, D.: Computational methods for plasticity: theory and applications. John Wiley & Sons, Ltd, 2008.
[10] Hertz, H.: Uber die beruhrung fester elastischer korper (on the contact of elastic solids). J. reine und angewandte Mathematik Vol.92, pp.156–171,1882
[11] Johnson, K.: Contact Mechanics, Cambridge University Press, 1985.
[12] Li, D., Wang, T., Cheng, T. and Sun, X.: Static and dynamic tensile failure characteristics of rock based on splitting test of circular ring, TNMSC, Vol.26, pp.1912–1918, 2016.
[13] Li, X., Feng, F. and Li, D..: Numerical simulation of rock failure under static and dynamic loading by splitting test of circular ring, Eng. Fract. Mech., Vol.188, pp.184–201, 2018.
[14] Kirishima, T.: Numerical simulation of geomaterials focusing on largedeformation problems using the material point method (in japanese), Shimizu Corporation research report, Vol.92, 2015.
[15] Cooper, M., Bromhead, E., Petley, D. and Grant, D.: The selborne cutting stability experiment, Geotechnique, Vol.48, pp.83–101, 1998.